*physchem*

MDPI

*Article*

# Phosphatidylinositol-4,5-biphosphate ($PIP_2$)-Dependent Thermoring Basis for Cold-Sensing of the Transient Receptor Potential Melastatin-8 (TRPM8) Biothermometer

**Guangyu Wang** [1,2]

[1] Department of Physiology and Membrane Biology, School of Medicine, University of California at Davis, Davis, CA 95616, USA; gary.wang10@gmail.com
[2] Department of Drug Research and Development, Institute of Biophysical Medico-Chemistry, Reno, NV 89523, USA

**Abstract:** The menthol sensor transient receptor potential melastatin-8 (TRPM8) can be activated by cold and, thus, serves as a biothermometer in a primary afferent sensory neuron for innocuous-to-noxious cold detection. However, the precise structural origins of specific temperature thresholds and sensitivity have remained elusive. Here, a grid thermodynamic model was employed, to examine if the temperature-dependent noncovalent interactions found in the 3-dimensional (3D) structures of thermo-gated TRPM8 could assemble into a well-organized fluidic grid-like mesh network, featuring the constrained grids as the thermorings for cold-sensing in response to $PIP_2$, $Ca^{2+}$ and chemical agents. The results showed that the different interactions of TRPM8 with $PIP_2$ during the thermal incubation induced the formation of the biggest grids with distinct melting temperature threshold ranges. Further, the overlapped threshold ranges between open and pre-open closed states were required for initial cold activation with the matched thermo-sensitivity and the decrease in the systematic thermal instability. Finally, the intact anchor grid near the lower gate was important for channel opening with the active selectivity filter. Thus, $PIP_2$-dependent thermorings in TRPM8 may play a pivotal role in cold sensing.

**Keywords:** grid thermodynamic model; lipid; noncovalent interaction; temperature sensitivity; thermoring; threshold



**Citation:** Wang, G. Phosphatidylinositol-4,5-biphosphate ($PIP_2$)-Dependent Thermoring Basis for Cold-Sensing of the Transient Receptor Potential Melastatin-8 (TRPM8) Biothermometer. *Physchem* **2024**, *4*, 106–119. https://doi.org/10.3390/physchem4020008

Academic Editor: Chih-Ching Huang

Received: 30 November 2023
Revised: 26 February 2024
Accepted: 22 March 2024
Published: 26 March 2024



## 1. Introduction

Transient receptor potential (TRP) melastatin-8 (TRPM8) is a $Ca^{2+}$-permeable ion channel. Its activation follows a Boltzmann-type relation, and its voltage activation range is dynamically regulated by temperature changes. It serves as a polymodal sensor, in response to both physical and chemical stimuli. The physical stimuli include membrane depolarization and cold, while the chemical stimuli cover the membrane phosphatidylinositol-4,5-biphosphate ($PIP_2$), lysophospholipids (LPLs) and the cooling agents, such as menthol, WS-12 and icilin [1–11]. When elevated temperature decreases the menthol-evoked activity of TRPM8, or menthol increases the temperature threshold and the maximal activity temperature of rat TRPM8 (rTRPM8) from 22–26 °C and 8.2 °C to 30–32 °C and 15.6 °C, respectively, the same gating pathway seems to be shared [1,2,12–18]. However, some menthol-sensitive residues, such as Y745 and Y1005 in mouse TRPM8 (mTRPM8), are insensitive to cold, challenging the same gating pathway [19,20]. On the other hand, the cold activation of TRPM8 exhibits a high temperature sensitivity $Q_{10}$ of 24–35 (the ratio of rates or open probabilities ($P_o$) of an ion channel measured 10 °C apart) at the physiological condition [11,12,21]. Although the cryo-electron microscopy (cryo-EM) structures of closed and open mTRPM8 at 20 °C are available in the absence or presence of $Ca^{2+}$, $PIP_2$ and chemical agents such as cryosim-3 (C3) and allyl isothiocyanate (AITC) [22], the precise structural factor or motif for the specific $PIP_2$-dependent cold temperature threshold and sensitivity is still missing.

Recent studies have demonstrated that a biological macromolecule has a thermoring structure to govern its thermal stability and activity. The thermoring can be a DNA hairpin in a single poly-nucleotide chain or a 3D topological grid in a systematic fluidic grid-like noncovalent interaction mesh network of a single polypeptide chain [23–28]. Such a biochemical or biophysical network can be characterized by a graph theory-based grid thermodynamic model. First, a melting temperature threshold ($T_m$) for the thermal unfolding of the thermoring from the biggest grid to the smallest one is determined by its strength and size. Second, the grid-based systematic thermal instability ($T_i$) at a specific temperature is governed by the ratio of the total grid size to the total noncovalent interactions. Third, the structural thermo-sensitivity ($\Omega_{10}$) is controlled by a change in the total grid sizes upon an alteration in the total noncovalent interactions along the same polypeptide chain within a 10 °C interval. Once three calculated parameters match the experimental values, including the functional thermo-sensitivity $Q_{10}$, the specific thermoring can be identified as the structural motif or factor for the structural thermostability or the functional thermoactivity [24–28]. Following a success in deciphering the lipid-dependent heat response and sensitivity of the TRP vanilloid 1 or 3 (TRPV1 or TRPV3) channel [27,28], it is attractive to use this graphical method to examine such a hypothesis that the temperature-dependent systematic fluidic grid-like noncovalent interaction mesh networks, once identified in the 3D structures of the TRPM8 channel, can be constrained as a thermoring structure from the biggest grid to the smallest one, to control the $PIP_2$-dependent cold-sensing with specific temperature threshold and sensitivity.

In this computational study, the three $PIP_2$-dependent biggest grids were first identified near the outer pore loop of mTRPM8. Their melting temperature threshold ranges in turn decreased upon the binding of the chemical agents C3 and AITC together with $Ca^{2+}$. Once the threshold matched the incubation temperature of 20 °C, the channel was open, with the intact anchor grid near the lower S6 gate to secure the active selectivity filter, the decrease in the systematic thermal instability and the matched structural and functional thermo-sensitivities. Taken as a whole, although TRPM8 can be finally opened by chemical agents in the presence of $Ca^{2+}$ and $PIP_2$, the $PIP_2$-dependent thermorings may still serve as the critical structural motif for cold-evoked activation of TRPM8 with the specific temperature threshold and sensitivity.

## 2. Materials and Methods

### *2.1. Data Mining Resources*

In this study, cryo-EM structural data of mTRPM8 in three gating states were exploited to prepare the systemic fluidic grid-like noncovalently interacting mesh networks. They included the closed states at 20 °C with $PIP_2$ bound (protein data bank (PDB) ID, 8E4N, model resolution = 3.07 Å) and with $PIP_2$, $Ca^{2+}$ and C3 bound (PDB ID, 8E4M, model resolution = 3.44 Å), and the open state at 20 °C with $PIP_2$, $Ca^{2+}$, C3 and AITC bound (PDB ID, 8E4L, model resolution = 3.32 Å) [22]. UCSF Chimera was used for the thermoring analyses.

### *2.2. The Definition of the Necessary Gating Pathway*

$PIP_2$ is required for TRPM8 opening [5,6,9,22]. The cryo-EM structure indicates that S4b, the TRP domain, and pre-S1 of mTRPM8 form the active $PIP_2$ binding pocket [22]. The primary structural analysis showed that mTRPM8 with $PIP_2$ bound at 20 °C (PDB ID, 8E4N) had F1013 in the distal C-terminus of the TRP domain to form a π–π interaction with F744 on S1. On the other hand, Q675 in the pre-S1 domain H-bonded with R998 in the TRP domain, in both closed and open states [22]. Hence, the segment from Q675 in the pre-S1 domain to F1013 in the distal C-terminus of the TRP domain should be at least included as the necessary minimal $PIP_2$-dependent gating pathway for the specific temperature threshold range and sensitivity and the reasonable systematic thermal instability.

### *2.3. Preparation of the Systematic Fluidic Noncovalent Interaction Mesh Network Maps*

For the thermoring structural analyses of a systematic fluidic grid-like mesh network of mTRPM8 along the $PIP_2$-dependent minimal gating pathway of one subunit, all the potential stereo- or regio-selective inter-domain diagonal and intra-domain lateral noncovalent interactions, such as salt/metal bridges and π interactions, and H-bonds, once filtered as described previously (Tables S1–S3), were geometrically mapped as grids [24–28]. By using the Floyd–Warshall algorithm, the grid size was constrained as the minimal number of the total side chains of free residues in protein or atoms in the bound lipid, which did not engage in any noncovalent interaction in a grid [29]. In this way, both the shortest direct and reverse paths were obtained to link two ends of a noncovalent interaction. For example, in Figure 1A, based on a grid-like biochemical reaction mesh network, a direct path length from F874 to Y908 was zero, owing to a π–π interaction between them. However, another shortest reverse path directed from Y908 to M878, W877 and back to F874 via three π interactions. Because no free residue participated in any noncovalent interaction during this cycle, the grid size was zero. Once each noncovalent interaction was tracked by a constrained grid size and the unshared sizes were marked in black numbers, a grid with an x-residue or atom size was denoted as $Grid_x$, and then all the noncovalent interactions and grid sizes along the $PIP_2$-dependent minimal gating pathway of one subunit were summed in black and cyan circles beside the mesh network map, respectively, for the computation of the melting temperature threshold ($T_m$), the systematic thermal instability ($T_i$) and the defined structural thermo-sensitivity ($\Omega_{10}$).

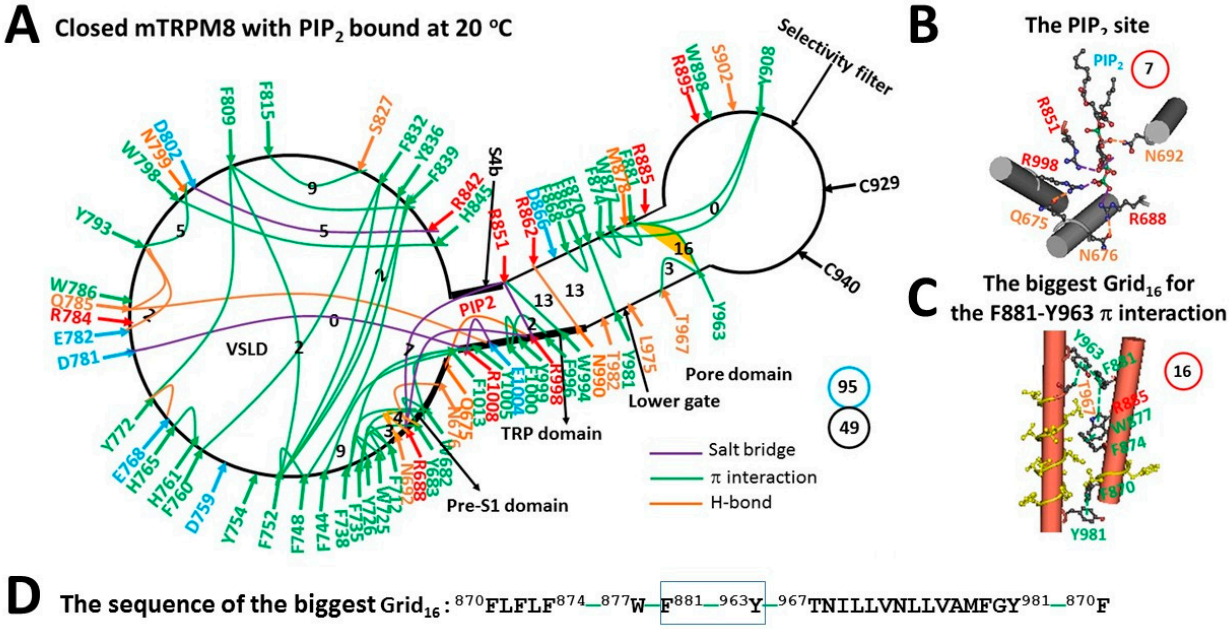


**Figure 1.** The grid-like non-covalently interacting mesh network along the $PIP_2$-dependent minimal gating pathway of closed mTRPM8 with $PIP_2$ bound at 20 °C. (**A**) The topological grids in the systemic fluidic grid-like mesh network. The cryo-EM structure of one subunit in homotetrameric closed mTRPM8 with $PIP_2$ bound at 20 °C (PDB ID, 8E4N) was used for the model. The pore domain, the selectivity filter, S4b, the TRP domain, the voltage sensor-like domain (VSLD) and the pre-S1 domain are indicated in black arrows. Salt bridges, π interactions and H-bonds between paired amino acid side chains along the $PIP_2$-dependent minimal gating pathway from Q675 to F1013 are marked in purple, green and orange, respectively. The grid sizes required to control the relevant noncovalent interactions were constrained with graph theory and labeled in black numbers. The F881–Y963 bridge in the biggest $Grid_{16}$ was highlighted. The calculated total grid sizes and noncovalent interactions are shown in the cyan and black circles, respectively. (**B**) The structure of the $PIP_2$ pocket. The grid size of the pocket is shown in a red circle. (**C**) The structure of the biggest $Grid_{16}$ at the S5/S6 interface. The grid size is shown in a red circle. (**D**) The sequence of the biggest $Grid_{16}$ to control the F881–Y963 π interaction in the blue box.

### *2.4. Equations*

When a 20-base loop and two G-C base pairs in the stem form a DNA hairpin thermosensor, an initial $T_m$ for loop unfolding is 34 °C, and then increased by 10 °C with a more G-C base pair or five more bases included [23]. Similarly, for the thermorings to undergo rate-limiting thermal unfolding from the biggest grid to the smallest one along the $PIP_2$-dependent minimal gating pathway, the $T_m$ of the given grid could be in turn calculated by using the following equation, as described and examined previously [24–28]:

$$T_m\ (^\circ C) = 34 + (n - 2) \times 10 + (20 - S_{max}) \times 2 \quad (1)$$

where n is the total number of the grid size-controlled basic H-bonds equivalent to the noncovalent interactions in a given grid, and $S_{max}$ is the size of the given grid. Clearly, a smaller grid size or more equivalent H-bonds are necessary for higher heat capacity in a grid.

Based on the above equation, the more G-C base pairs in the stem or the shorter poly-A loop, the higher the $T_m$ of the DNA hairpin [23]. Thus, in either gating state, the systematic thermal instability ($T_i$) along the $PIP_2$-dependent minimal gating pathway was reasonably defined using the following equation, as described and examined previously [24–28]:

$$T_i = S/N \quad (2)$$

where along the same $PIP_2$-dependent minimal gating pathway of one subunit in a given gating state, S is the total grid sizes and N is the total noncovalent interactions. In this way, the lower the $T_i$, the less the compact conformational entropy in the system.

In a temperature range ΔT, for an enthalpy-driven closed-to-open transition, assuming the chemical potential of a grid as the maximal potential for equivalent residues in the grid to form the tightest β-hairpin with the smallest loop via paired noncovalent interactions [30], the grid-based structural thermo-sensitivity ($\Omega_{\Delta T}$) of a single ion channel can be defined and computed using the following equations:

$$\Omega_{\Delta T} = -[(S_c - S_o)E/2]^{(Hc/Ho)} = -[(S_c - S_o)E/2]^{[(ENc)/(ENo)]} = -[(S_c - S_o)E/2]^{(Nc/No)} \quad (3)$$

where, along the same $PIP_2$-dependent minimal gating pathway of one subunit, $N_c$ and $N_o$ are the total noncovalent interactions, $S_c$ and $S_o$ are the total grid sizes, and $H_c$ and $H_o$ are the total enthalpy included in noncovalent interactions in the closed and open states, respectively. E is the energy strength of a noncovalent interaction in a range of 0.5–3 kcal/mol. Usually, E is 1 kcal/mol [31]. Thus, $\Omega_{\Delta T}$ actually mirrors a thermo-induced change in the total chemical potential of grids upon a thermo-evoked change in the total enthalpy included in noncovalent interactions from a closed state to an open one along the same $PIP_2$-dependent minimal gating pathway of one subunit.

When ΔT = 10 °C, $\Omega_{10}$ could be comparable to the functional thermo-sensitivity ($Q_{10}$) of a single ion channel. $Q_{10}$ during thermal activation was computed using the following equation:

$$Q_{10} = -(X_2/X_1)^{10/(T_1 - T_2)} \quad (4)$$

where $X_1$ and $X_2$ are open probability ($P_o$) values or reaction rates of mTRPM8 at temperatures $T_1$ and $T_2$ (measured in kelvin), respectively.

## 3. Results

### *3.1. Identification of a Phosphatidylinositol-4,5-biphosphate ($PIP_2$)-Dependent Cooling Switch at 32–37 °C in Mouse Transient Receptor Potential Melastatin-8 (mTRPM8)*

For a given $PIP_2$-dependent minimal gating pathway from Q675 in the pre-S1 domain to F1013 in the distal C-terminus of the TRP domain of mTRPM8 at 20 °C, nine H-bonds, thirty-four π interactions and six salt bridges shaped a systematic fluidic grid-like mesh network (Figure 1A). When the total noncovalent interactions and grids size were 49 and

95, respectively (Figure 1A, Table S1), the grid-based systematic thermal instability ($T_i$) was 1.94 (Table 1).

**Table 1.** New $PIP_2$-dependent parameters of the TRPM8 bio-thermometer, based on the grid thermodynamic model. The comparative parameters are highlighted in bold.

| **Construct** | **mTRPM8** | | |
|---|---|---|---|
| PDB ID | 8E4L | 8E4M | 8E4N |
| $Ca^{2+}$ | bound | bound | free |
| $PIP_2$ | bound | bound | bound |
| Sampling temperature, °C | 20 | 20 | 20 |
| Gating state | open | closed | closed |
| Name of the biggest grid | $Grid_{22}$ | $Grid_{21}$ | $Grid_{16}$ |
| Biggest grid size ($S_{max}$) | 22 | 21 | 16 |
| Equivalent basic H-bonds to control $S_{max}$ | 1.0–1.5 | 1.0–1.5 | 1.0–1.5 |
| Total noncovalent interactions | 51 | 49 | 49 |
| Total grid sizes, a. a./atoms | 74 | 93 | 95 |
| Systematic thermal instability ($T_i$) | 1.45 | 1.90 | 1.94 |
| Calculated $T_m$, °C | **20–25** | **22–27** | **32–37** |
| Measured threshold $T_{th}$, °C | **23–29** | **23–29** | **31–37** |
| Calculated $\Omega_{10,\,min}$ at E = 0.5 kcal/mol | | −4.46 | |
| Calculated $\Omega_{10,\,mean}$ at E = 1.0 kcal/mol | | **−8.68** | |
| Calculated $\Omega_{10,\,max}$ at E = 3.0 kcal/mol | | −24.9 | |
| Measured $Q_{10}$ | | **−9.16** | |
| Ref. for measured $T_{th}$ and $Q_{10}$ | [5] | [5] | [5] |

Notably, in the presence of 1 mM $PIP_2$ [22], $PIP_2$ was packaged by R688 and N692 in the pre-S1, R851 at S4b, and R998 in the TRP domain via three salt bridges and an H-bond (Figure 1B). In this case, the biggest $Grid_{16}$ was outstanding at the S5/S6 interface. It had a 16-residue size via the shortest path from F881 to Y963, T967, Y981, F870, F874, W877 and back to F881 (Figure 1C). When 1.0–1.5 equivalent H-bonds sealed this biggest $Grid_{16}$ to hold the F881–Y963 π interaction at the S5/S6 interface (Figure 1C), the calculated melting temperature threshold ($T_m$) ranged from 32 to 37 °C, which was close to the experimental threshold range of 31–37 °C of mTRPM8 for cold activation in the presence of a high concentration of $PIP_2$ (>500 μM) [5]. Thereafter, the biggest $Grid_{16}$ may act as a start cooling switch in TRPM8 to initiate channel activation in an optimal temperature range 32–37 °C. However, it could not be broken at 20 °C for channel opening [22].

### *3.2. Addition of $Ca^{2+}$ and Cooling Agent cryosim-3 (C3) Decreased the Activation Threshold Range of Mouse Transient Receptor Potential Melastatin-8 (mTRPM8) to 22–27 °C*

It has been reported that $Ca^{2+}$ binding cannot change the temperature threshold for cold-evoked activation of mTRPM8 [32]. On the other hand, the C3-evoked TRPM8 activity at room temperature (22–24 °C) is not desensitized by $Ca^{2+}$ [22]. However, mTRPM8 is not structurally open in the presence of C3, $Ca^{2+}$ and $PIP_2$ at 20 °C [22]. Therefore, it is necessary to test the effect of C3 on the activation threshold of mTRPM8. When $Ca^{2+}$ bridged E782, Q785, N799 and D802 together, the Y793–N799 π interaction and the E782–Y793–Q785 H-bonds were broken (Figures 1A and 2A). Although C3 was bound against Y745 in the voltage sensor-like domain (VSLD) [22], it did not link any two residues together via a noncovalent interaction (Figure 2A). In contrast, the R851–$PIP_2$ salt bridge was replaced with the S850–$PIP_2$ H-bond (Figure 2B). As a result, when the total noncovalent interactions

and grid sizes were 49 and 93, respectively, the resultant systematic thermal instability ($T_i$) decreased from 1.94 to 1.90 (Figure 2A, Table 1). What is more, the biggest $Grid_{21}$ appeared at the S5/S6 interface to control the F881–T967 H-bond. It had a 21-residue size via the shortest path from F881 to W877, F874, F870, F869, D866, Y981, T967 and back to F881 (Figure 2C,D). With 1.0–1.5 equivalent H-bonds sealing it, the calculated melting temperature threshold range was 22–27 °C, which was close to the experimental range of 23–29 °C in the presence of 100 μM $PIP_2$ [5]. However, it was still higher than the sampling temperature 20 °C of the structural data, thereby leaving the channel closed [22].

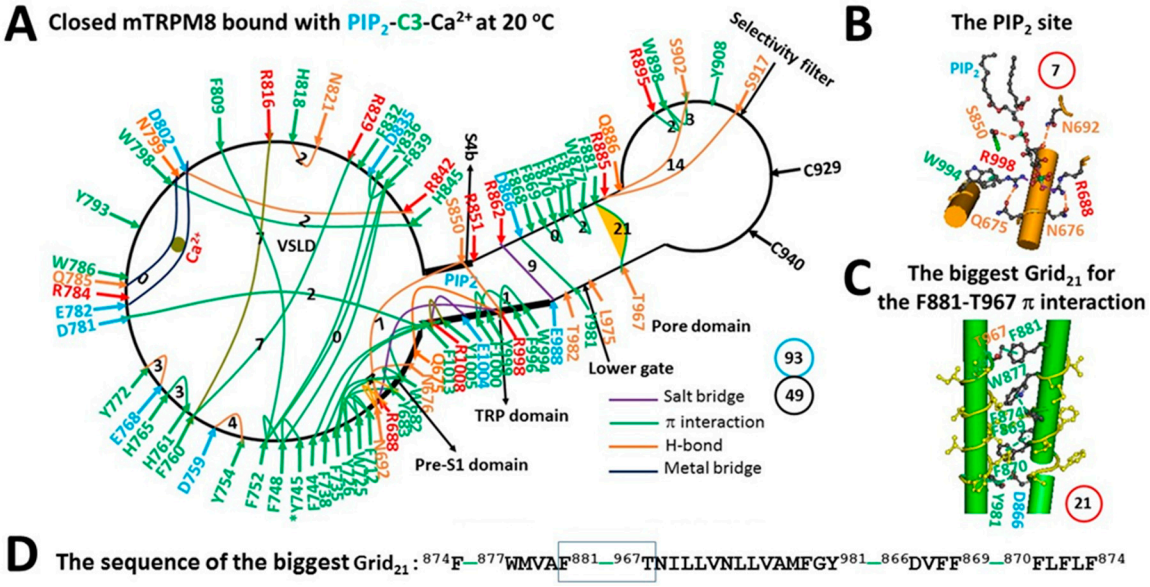


**Figure 2.** The grid-like noncovalently interacting mesh network along the $PIP_2$-dependent minimal gating pathway of closed mTRPM8 with $Ca^{2+}$, $PIP_2$ and C3 bound at 20 °C. (**A**) The topological grids in the systemic fluidic grid-like mesh network. The cryo-EM structure of one subunit in homotetrameric closed mTRPM8 with $Ca^{2+}$, $PIP_2$ and C3 bound at 20 °C (PDB ID, 8E4M) was used for the model. The C3 binding residue (Y745) is marked by an asterisk. The pore domain, the selectivity filter, S4b, the TRP domain, the VSLD and the pre-S1 domain are indicated in black arrows. Salt bridges, π interactions, H-bonds and metal bridges between paired amino acid side chains along the $PIP_2$-dependent minimal gating pathway from Q675 to F1013 are marked in purple, green, orange and blue, respectively. The grid sizes required to control the relevant noncovalent interactions were constrained with graph theory and labeled in black numbers. The F881–T967 π bridge in the biggest $Grid_{21}$ was highlighted. The calculated total grid sizes and noncovalent interactions are shown in the cyan and black circles, respectively. (**B**) The structure of the $PIP_2$ binding site. The grid size of the pocket is shown in a red circle. (**C**) The structure of the biggest $Grid_{21}$ at the S5/S6 interface. The grid size is shown in a red circle. (**D**) The sequence of the biggest $Grid_{21}$ to control the F881–T967 π interaction in the blue box.

### *3.3. Further Addition of allyl isothiocyanate (AITC) Opened Mouse Transient Receptor Potential Melastatin-8 (mTRPM8) at the Matched Threshold of 20 °C*

In the presence of not only $Ca^{2+}$, $PIP_2$ and C3 but also AITC at 20 °C, mTRPM8 was open with several changes in the systematic fluidic grid-like noncovalent interaction mesh network (Figure 3A). First, at the $Ca^{2+}$ site, W786–Y793–W798 π interactions and the Y793–E782 and D781–R784 H-bonds were formed. Second, C3 and AITC were bound against Y745 and W798 in the VSLD, respectively [22]. However, these two chemical agonists failed to connect any two residues together via a noncovalent interaction (Figure 3A). Third, $PIP_2$ was bound again to R688, R851 and R998, forming a $Grid_7$ (Figure 3B). Fourth, along with the $PIP_2$ binding, the D781–F1013 π interaction was disrupted to allow the gating $Grid_8$ to be born with an 8-residue size via the shortest path from H845 to R851, W994, R998, Y999, F1000, E1004 and back to H845 (Figure 3A,D). Fifth, when R851 formed a π interaction

with W994 and an H-bond with D991 in the TRP domain, the D866–T982 H-bond and the F870–L975 π interaction at the S5/S6 interface were created to form the thermo-stable anchor $Grid_7$ in favor of the active lower S6 gate (Figure 3A). It had a 7-residue size from D866 to F868, F869, F870, L975, T982 and back to D866 (Figure 3D). Meanwhile, the biggest $Grid_{22}$ in the pore domain had a 22-residue size to stabilize the open state via the shortest path from F874, W877, F881, Y963, R885, Y908 and back to F874 (Figure 3C,D). When 1.0–1.5 equivalent H-bonds sealed it, the calculated $T_m$ ranged from 20 to 25 °C, which matched the sampling temperature 20 °C of the open state [22]. As the total noncovalent interactions and grids size were 51 and 74, respectively (Figure 3A, Table S3), the grid-based systematic thermal instability ($T_i$) further decreased to 1.45 (Table 1). For channel opening upon the addition of AITC, the calculated mean $\Omega_{10}$ of −8.68 was close to the experimental $Q_{10}$ of −9.16 at 100 μM $PIP_2$ (Table 1) [5].

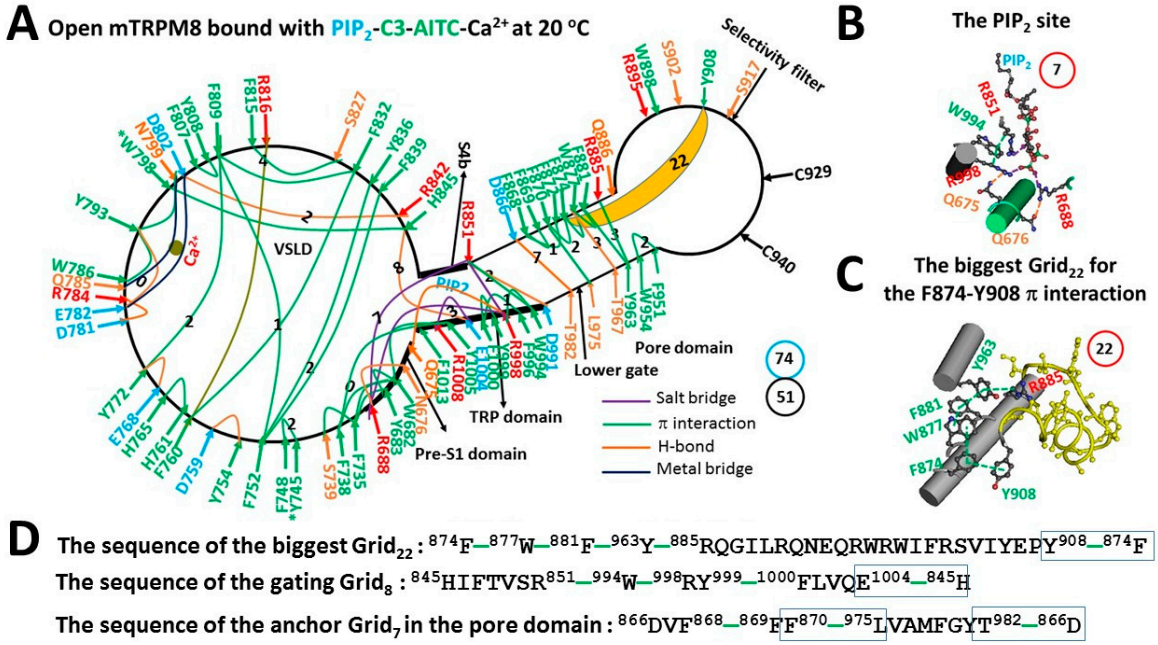


**Figure 3.** The grid-like noncovalently interacting mesh network along the $PIP_2$-dependent minimal gating pathway of open mTRPM8 with $Ca^{2+}$, $PIP_2$, C3 and AITC bound at 20 °C. (**A**) The topological grids in the systemic fluidic grid-like mesh network. The cryo-EM structure of one subunit in homotetrameric open mTRPM8 with $Ca^{2+}$, $PIP_2$, C3 and AITC bound at 20 °C (PDB ID, 8E4L) was used for the model. The C3 binding residue (Y745) and the AITC binding residue (W798) are marked by asterisks. The pore domain, the selectivity filter, S4b, the TRP domain, the VSLD and the pre-S1 domain are indicated in black arrows. Salt bridges, π interactions, H-bonds and metal bridges between paired amino acid side chains along the $PIP_2$-dependent minimal gating pathway from Q675 to F1013 are marked in purple, green, orange and blue, respectively. The grid sizes required to control the relevant non-covalent interactions were constrained with graph theory and labeled in black numbers. The F874–Y908 bridge in the biggest $Grid_{22}$ at 20 °C was highlighted. The calculated total grid sizes and noncovalent interactions are shown in the cyan and black circles, respectively. (**B**) The structure of the $PIP_2$ binding site. The grid size of the pocket is shown in a red circle. (**C**) The structure of the biggest $Grid_{22}$ in the pore domain. The grid size is shown in a red circle. (**D**) The sequence of the biggest $Grid_{22}$ to control the F874–Y908 π interaction in the blue box; the sequence of the gating $Grid_8$ to control the H845–E1004 H-bond in the blue box; and the sequence of the anchor $Grid_7$ in the pore domain to control the D866–T982 H-bond and the F870–L975 π interaction in the blue boxes.

## 4. Discussion

The release of the lipid phosphatidylcholine (PC) or phosphatidylinositol (PI) from the vanilloid site of TRPV3 or TRPV1 is required for heat activation, respectively [33,34]. In contrast, the cold activation of TRPM8 needs the lipid $PIP_2$ [5,6,9,22]. Although the role of PC or PI in heat response and sensitivity of TRPV3 or TRPV1 has been illuminated recently [27,28], much less is known about how the interaction of TRPM8 with $PIP_2$ governs the specific temperature threshold and sensitivity for cold sensing. In this computational study, the three $PIP_2$-dependent biggest grids at or near the S5/S6 interface of mTRPM8 were identified in the presence of the high concentration of 1 mM $PIP_2$. Further studies showed that the different interactions of mTRPM8 with $PIP_2$, in response to the addition of $Ca^{2+}$ and the chemical agents C3 and AITC, created declined melting temperature threshold ranges, which were calculated from those $PIP_2$-dependent biggest grids. When two threshold ranges in both open and pre-open closed states were similar, the channel could be opened with the matched thermosensitivity and the decrease in the systematic thermal instability. Finally, the intact anchor near the lower gate was necessary for channel opening with the active selectivity filter. Therefore, this study may promote our understanding about the role of the lipids in regulating distinct thermorings for specific temperature thresholds and sensitivity in thermo-gated TRP channels.

### *4.1. Interaction of Transient Receptor Potential Melastatin-8 (TRPM8) with Phosphatidylinositol-4,5-biphosphate ($PIP_2$) Determined the Temperature Threshold Range for Channel Opening*

The temperature threshold ranges increased from 23–29 °C to 31–37 °C when the concentration of $PIP_2$ raised from 0.1 to 0.5 mM [5]. However, the underlying structural motif is unknown. This computational study identified two biggest grids in the systemic fluidic grid-like noncovalently interacting mesh networks of mTRPM8 in the presence of 1 mM $PIP_2$. In the absence of the cooling agent C3, $PIP_2$ was found tightly bound with R688 and N692 in the pre-S1 domain, R851 at S4b, and R998 in the TRP domain via three salt bridges or one H-bond (Figure 1B). In this case, the biggest $Grid_{16}$ at the S5/S6 interface generated the calculated melting temperature threshold range from 32 to 37 °C, which was similar to the measured activation threshold range from 31 to 37 °C (Table 1) [5]. In the presence of the cooling agent C3, the salt bridge between R851 and $PIP_2$ was substituted by the S850-$PIP_2$ H-bond (Figure 2B). In that case, another biggest $Grid_{21}$ at the S5/S6 interface had the calculated melting temperature threshold range from 22 to 27 °C, which was close to the experimental threshold range from 23 to 29 °C (Table 1) [5]. Thus, it is possible that $PIP_2$ may have a similar interaction with TRPM8 for the biggest $Grid_{21}$ to be a temperature sensor in the pore domain when the concentration declines to 0.1 mM.

On the other hand, the temperature sensation of mammalian TRPM8 is reportedly regulated by the initial or ambient temperature [32]. For example, the rise in the exposed temperature from 30 to 40 °C can increase the temperature threshold for the activation of human or rat TRPM8 (hTRPM8 or rTRPM8, respectively) from 28.3 °C to 33.8 °C in *HEK293* cells expressing hTRPM8 [32]. Furthermore, reducing the level of cellular $PIP_2$ or the R1008Q mutation in the TRP domain attenuates or eliminates the ambient temperature-induced changes in the cold temperature threshold [32]. Therefore, the interaction of TRPM8 with $PIP_2$ plays a pivotal role in modifying the temperature threshold for channel activation. At the ambient temperature 40 °C, the higher level of cellular $PIP_2$ may allow the tight interaction at the pre-S1/S4b/TRP interfaces to produce the biggest $Grid_{16}$ or the similar one with a higher temperature threshold 33.8 °C (Figure 1B,D, Table 1). In contrast, at lower pre-determined temperature 30 °C, cellular $PIP_2$ may decrease the level so that the relatively loose binding to the pre-S1/S4b/TRP interfaces could trigger the formation of another biggest $Grid_{21}$ or the similar one with the lower threshold of 28.3 °C (Figure 2B,D, Table 1). In good agreement with this proposal, in the former case, R1008 in the TRP domain interacted with both D781 in the VSLD and nearby E1004 via the salt bridges (Figure 1A). However, in the latter case, the D781–R1008 salt bridge was replaced by the D781–F1013 $\pi$

interaction (Figure 2A). Thereafter, the R1008Q mutation may allow the loose binding of $PIP_2$ to TRPM8 to have a similar lower threshold for channel activation, no matter whether the exposed temperature increased from 30 to 40 °C [32]. Since the cellular $PIP_2$ level did decline upon a temperature decrease from 25 to 10 °C [35], it is reasonable that the open state of TRPM8 could be stabilized at the maximal activity temperature of 8.2 °C [1,2]. In that case, the stimulatory H-bond between H845 in the VSLD and E1004 in the TRP domain may be enough to allow the gating $Grid_8$ to hold the open state even at the lower $PIP_2$ level once TRPM8 has been activated (Figure 3A,D).

### *4.2. Implication of Transient Receptor Potential Melastatin-8 (TRPM8) Activation by Lysophospholipids (LPLs) and Menthol*

In addition to $PIP_2$, a small dose (3 μM) of long-chain intracellular LPLs can also directly activate TRPM8 even at normal body temperature. This activation has prominent prolongation of channel openings and can be suppressed by protons at pH 6 but not by $Mg^{2+}$ [10,11]. In this case, $PIP_2$ may not be involved, so that either or both of free $PIP_2$ and AITC sites may hold LPLs with smaller head groups, stabilizing the stimulatory interaction between S4b and the TRP domain for channel opening at elevated temperature (Figure 3B) [6,22].

In contrast, menthol may share the same pocket with C3. The binding of a single menthol molecule to R841 on S4 has been proposed to stimulate TRPM8 activity [36]. However, that model cannot explain the Y1005-dependent menthol upregulation of TRPM8 with a low efficacy but a high coefficient of a dose response at membrane hyperpolarization [19,37,38], and the ligand stereoselectivity of the LNI1009PAA mutant [19]. Thus, in addition to H-bonding with R841, an H-bonded homochiral menthol dimer with head-to-head or head-to-tail is still required to push Y1005 against the anchors L841 and I844 on S4 of mTRPM8 for those experimental observations [20]. In this way, the tighter interaction between $PIP_2$ and TRPM8 may be allowed to increase the melting temperature threshold for channel opening. Further structural data are necessary to reveal the LPLs or menthol sites and their roles in stimulating TRPM8 opening at higher temperature.

### *4.3. Overlapped Temperature Thresholds between Open and Pre-Open Closed States Were Required for Cold-Sensing*

The open state of mTRPM8 in the presence of high concentration of $PIP_2$ at 20 °C had the biggest $Grid_{22}$ for the melting temperature threshold range of 20–25 °C (Figure 1, Table 1). Therefore, even if the channel can be opened at 32–37 °C in the presence of 0.5 mM $PIP_2$ [5], the biggest $Grid_{22}$ would have melted at 32–37 °C and, hence, another biggest grid may be necessary to match the higher $T_m$ of 32–37 °C for channel opening. In contrast, the pre-open closed state of mTRPM8 with $Ca^{2+}$ and C3 bound in the presence of 1 mM $PIP_2$ had the biggest $Grid_{21}$ for the calculated $T_m$ range from 22 to 27 °C (Figure 2C,D). Therefore, the biggest $Grid_{22}$ in the open state could adapt a temperature range from 22 to 25 °C even if AITC was absent (Figure 4). In other words, the overlapped thresholds between open and pre-open closed states may be necessary for cold activation of TRPM8. Given that the threshold is 25 °C at the cellular $PIP_2$ concentration of 10 μM [5,39], further structural investigations of closed and open mTRPM8 at 10 μM $PIP_2$ around 25 °C may be required for the detailed understanding about how the TRPM8 bio-thermometer senses cold under the native physiological condition.

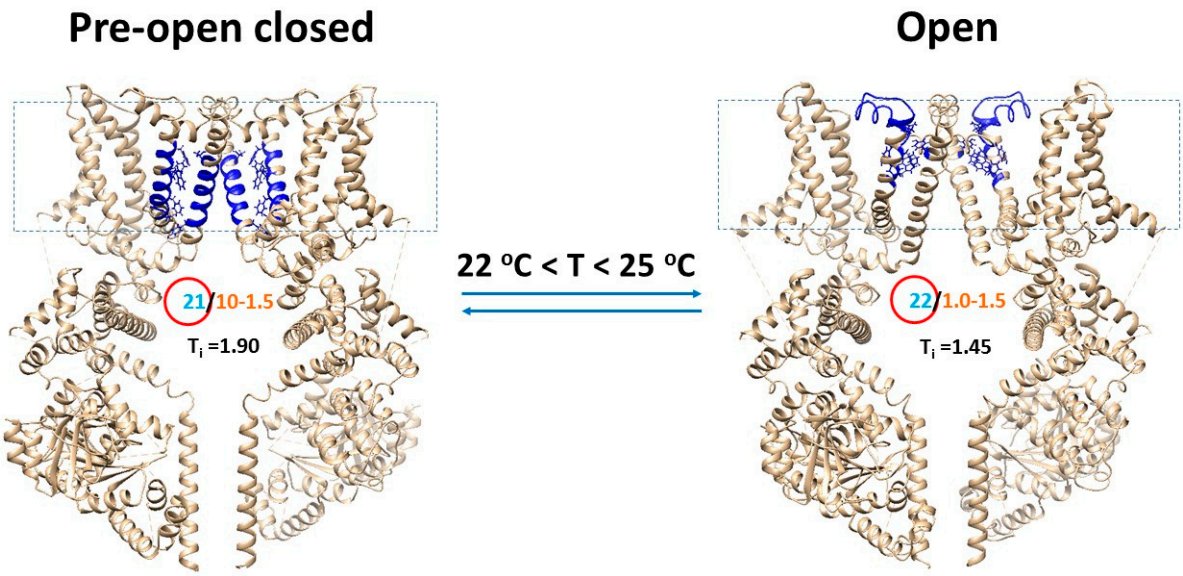


**Figure 4.** Tentative cold switches in the TRPM8 biothermometer. A, the homo-tetrameric cryo-EM structure of mTRPM8 with (PDB ID, 8E4L) or without (PDB ID, 8E4M) AITC bound in the presence of $Ca^{2+}$, $PIP_2$ and C3 at 20 °C was used for the model of the open or pre-open closed state, respectively. For convenience, only two opposite subunits are shown. The dashed rectangle is the membrane area. The $PIP_2$-dependent biggest $Grid_{21}$ in the pre-open closed state and the biggest $Grid_{22}$ in the open state have the overlapped $T_m$ range of 22–25 °C for channel opening with the matched temperature threshold range and sensitivity (Table 1). The grid sizes (cyan) are shown in the red circles, along with equivalent basic H-bond numbers (orange) to control them.

### *4.4. Thermostable F874–Y908 π Interaction in the Pore Domain Was Needed for the Active Selectivity Filter*

A previous chimera study of TRPM8 in a cold-sensitive mouse, rat or African elephant versus a cold-insensitive squirrel, hamster, chicken or emperor penguin showed that the outer pore loop is thermosensitive [40–42]. Notably, the R897E mutation in mTRPM8 inhibits the cold response but does not alter the menthol response [41]. Further, the Y908A mutation, rather than the Y908W/F mutation, in the P-helix suppresses the cold-sensing, although their response to icilin or menthol is not affected [43]. Because Y908 is close to the selectivity filter [22], this residue is crucial for the cold-evoked activity. This study indicated that the F874–Y908 π interaction was highly conserved in both closed and open states (Figures 1A and 3A, Tables S1 and S3). In this regard, such a π interaction may be required to secure the active selectivity filter, although the segment from Y925 to P950 of the outer pore loop was unstructured in both closed and open states in the absence of the C929-C940 disulfide bond (Figures 1A–3A) [22,44].

### *4.5. Thermostable Anchor $Grid_7$ at the S5/S6 interface Was Necessary for the Active Lower S6 Gate*

D866, T982, F870, and L975 are highly conserved in thermosensitive TRPM2-5 and TRPV1-4 [22,33]. The equivalent T680A mutation (T982 in mTRPM8) has been reported to suppress heat activation of TRPV3 [45]. Moreover, both equivalent D576–T680 H-bond and F590–L673 π interaction in rTRPV1, or both equivalent D586–T685 H-bond and F580–L678 π interaction in mTRPV3, are always highly conserved in a thermo-stable anchor grid in both closed and open states [27,28]. On the other hand, L975 is close to the lower S6 gate of mTRPM8 [22,44]. Accordingly, the D866–T982 H-bond and the F870–L975 π interaction in the anchor $Grid_7$ at the S5/S6 interface may be required to secure the active lower S6 gate of mTRPM8 (Figure 3A,D). In consonance with this proposal, the Y981F mutation near T982 in rTRPM8 is not functional but the Y981K/E mutation destabilizes the lower gate, rendering rTRPM8 constitutively active [46]. Since these two noncovalent interactions only appeared in the open state of mTRPM8 (Figure 3A,D), the gating rearrangement at

the temperature threshold may be necessary to keep the intact anchor $Grid_7$ at the S5/S6 interface for channel opening with the active selectivity filter.

### *4.6. Transient Receptor Potential Melastatin-8 (TRPM8) Opened with the Matched Thermosensitivity and the Decrease in the Systematic Thermal Instability*

Although the cold sensitivity of TRPM8 in response to a native $PIP_2$ environment is high ($Q_{10}$, 24–35) [11,12,21,32], the calculated structural thermosensitivity for channel opening from the pre-open closed state, upon the addition of the chemical agent AITC, was still lower in the presence of 1 mM $PIP_2$ ($\Omega_{10}$, −8.68) (Table 1). As this value was similar to the experimental $Q_{10}$ of −9.16 at 0.1 mM $PIP_2$ or the temperature coefficient ($Q_{10}$, 9) of the rundown rate of cold response upon excision of the membrane patch into the $PIP_2$-free bath solution [5,6], the physiological $PIP_2$ concentration for the cold detection of TRPM8 may be dynamic [6,9]. On the other hand, although a simple two-state model or an allosteric model has been proposed for single-channel gating mechanisms of TRPM8 activation by cold and membrane depolarization [13,21], a more complex seven-state model may be needed for the high temperature sensitivity of TRPM8 [47], which cannot be figured out by two closed states and one open state in this study. In fact, in addition to the VSLD [40], the side-chain hydrophobicity in the pore domain has been shown to play a critical role in the thermosensitivity of TRPM8 in different vertebrates [42]. However, the segment from Y925 to P950 of the outer pore loop in these three states were mostly unstructured (Figures 1A–3A). Hence, the alteration in the heat capacity as a result of the changes in not only the total grid sizes along the $PIP_2$-dependent minimal gating pathway but also the side-chain hydrophobicity in the pore domain, along with multiple gating transitions, may be required for such high temperature sensitivity. In addition, recent behavioral studies have shown that phosphoinositide-interacting regulator of TRPs (PIRT) can bind to $PIP_2$ and is required for normal TRPM8-mediated cold-sensing [48]. Therefore, further structural and functional examinations of the $PIP_2$-dependent thermosensitivity, with or without PIRT bound along with the hydrophobic or hydrophilic change in the pore domain, are expected under the physiological condition.

In any way, it is interesting that the similar decrease in the systematic thermal instability ($T_i$, from 1.90 to 1.45) was observed upon cold-evoked TRPM8 opening just it was as heat-evoked TRPV1 opening ($T_i$, from 1.91 to 1.65) or TRPV3 opening ($T_i$, from 1.88 to 1.20) [27,28]. In that regard, the thermo-gated TRP channel opening may be driven by the minimization of the systematic thermal instability. Further cross-examinations of other thermo-sensitive TRP channels may be required.

## 5. Closing Remark

The TRPM8 channel can be activated by either cold or chemical agents such as C3 and AITC. This computational study demonstrated that both physical and chemical stimuli may share a similar gating pathway. Although $Ca^{2+}$ binding was not necessary, $PIP_2$ was required to induce the stimulatory interaction at the pre-S1/voltage sensor/TRP domain interfaces. Further, the overlapped thresholds between open and pre-open closed states may favor the cold-evoked channel activation. Finally, the intact thermal anchor grid near the lower gate was required to secure the active selectivity filter for channel opening. Accordingly, this study may provide important clues as to how the TRPM8 biothermometer uses the $PIP_2$-dependent thermorings, from the biggest grids to the smallest ones, to achieve innocuous-to-noxious cold detection with specific matched temperature thresholds and sensitivity. This study further confirmed the existence of a lipid-dependent temperature sensor in thermo-gated TRP channels. The proposed mechanisms and thermoring concept in this study may facilitate our understanding of the activation of TRPM8 by lysophospholipids and menthol.

**Supplementary Materials:** The following supporting information can be downloaded at: https://www.mdpi.com/article/10.3390/physchem4020008/s1, Table S1: Noncovalent interactions along the $PIP_2$-dependent minimal gating pathway from Q675 to F1013 in each subunit of closed mTRPV8 with $PIP_2$ bound at 20 °C (PDB ID, 8E4N); Table S2: Noncovalent interactions along the $PIP_2$-dependent minimal gating pathway from Q675 to F1013 in each subunit of closed mTRPM8 with $Ca^{2+}$ and $PIP_2$ and C3 bound at 20 °C (PDB ID, 8E4M); Table S3: Noncovalent interactions along the $PIP_2$-dependent minimal gating pathway from Q675 to F1013 in each subunit of open mTRPM8 with $Ca^{2+}$ and $PIP_2$ and chemical agents C3 and AITC bound at 20 °C (PDB ID, 8E4L).

**Funding:** This research was initiated by the American Heart Association Grant (10SDG4120011 to GW).

**Data Availability Statement:** All data generated or analyzed during this study are included in this published article.

**Conflicts of Interest:** The author declares no conflicts of interest.

## Abbreviations

AITC, allyl isothiocyanate; C3, cryosim-3 or 1-diisopropylphosphorylnonane; cryo-EM, cryo-electron microscopy; $Q_{10}$, functional thermo-sensitivity; LPLs, lysophospholipids; $T_m$, melting temperature threshold; $P_o$, open probability; $\Omega_{10}$, structural thermo-sensitivity; PC, phosphatidylcholine; PI, phosphatidylinositol; $PIP_2$, phosphatidylinositol-4,5-bisphosphate; PIRT, phosphoinositide-interacting regulator of TRPs; $T_i$, systematic thermal instability; TRP, transient receptor potential; TRPM8, TRP melastatin-8; cTRPM8, chicken TRPM8; hTRPM8, human TRPM8; mTRPM8, mouse TRPM8; rTRPM8, rat TRPM8; VSLD, voltage-sensor-like domain; WS-12, N-(4-methoxyphenyl)-p-menthone-3-carboxamide.

## References

1. McKemy, D.D.; Neuhausser, W.M.; Julius, D. Identification of a cold receptor reveals a general role for TRP channels in thermosensation. *Nature* **2002**, *416*, 52–58. [CrossRef] [PubMed]
2. Peier, A.M.; Moqrich, A.; Hergarden, A.C.; Reeve, A.J.; Andersson, D.A.; Story, G.M.; Earley, T.J.; Dragoni, I.; McIntyre, P.; Bevan, S.; et al. A TRP channel that senses cold stimuli and menthol. *Cell* **2002**, *108*, 705–715. [CrossRef]
3. Reid, G.; Babes, A.; Pluteanu, F. A cold- and menthol-activated current in rat dorsal root ganglion neurones: Properties and role in cold transduction. *J. Physiol.* **2002**, *545*, 595–614. [CrossRef] [PubMed]
4. Chuang, H.-H.; Neuhausser, W.M.; Julius, D. The super-cooling agent icilin reveals a mechanism of coincidence detection by a temperature-sensitive TRP channel. *Neuron* **2004**, *43*, 859–869. [CrossRef]
5. Rohács, T.; Lopes, C.M.B.; Michailidis, I.; E Logothetis, D. PI(4,5)P2 regulates the activation and desensitization of TRPM8 channels through the TRP domain. *Nat. Neurosci.* **2005**, *8*, 626–634. [CrossRef]
6. Liu, B.; Qin, F. Functional control of cold- and menthol-sensitive TRPM8 Ion channels by phosphatidylinositol 4,5-bisphosphate. *J. Neurosci.* **2005**, *25*, 1674–1681. [CrossRef]
7. Voets, T.; Owsianik, G.; Janssens, A.; Talavera, K.; Nilius, B. TRPM8 voltage sensor mutants reveal a mechanism for integrating thermal and chemical stimuli. *Nat. Chem. Biol.* **2007**, *3*, 174–182. [CrossRef] [PubMed]
8. Bödding, M.; Wissenbach, U.; Flockerzi, V. Characterisation of TRPM8 as a pharmacophore receptor. *Cell Calcium* **2007**, *42*, 618–628. [CrossRef]
9. Zakharian, E.; Cao, C.; Rohacs, T. Gating of transient receptor potential melastatin 8 (TRPM8) channels activated by cold and chemical agonists in planar lipid bilayers. *J. Neurosci.* **2010**, *30*, 12526–12534. [CrossRef]
10. Abeele, F.V.; Zholos, A.; Bidaux, G.; Shuba, Y.; Thebault, S.; Beck, B.; Flourakis, M.; Panchin, Y.; Skryma, R.; Prevarskaya, N. $Ca^{2+}$-independent phospholipase A2-dependent gating of TRPM8 by lysophospholipids. *J. Biol. Chem.* **2006**, *281*, 40174–40182. [CrossRef]
11. Andersson, D.A.; Nash, M.; Bevan, S. Modulation of the cold-activated channel TRPM8 by lysophospholipids and polyunsaturated fatty acids. *J. Neurosci.* **2007**, *27*, 3347–3355. [CrossRef] [PubMed]
12. Andersson, D.A.; Chase, H.W.N.; Bevan, S. TRPM8 activation by menthol, icilin, and cold Is differentially modulated by intracellular pH. *J. Neurosci.* **2004**, *24*, 5364–5369. [CrossRef]
13. Voets, T.; Droogmans, G.; Wissenbach, U.; Janssens, A.; Flockerzi, V.; Nilius, B. The principle of temperature-dependent gating in cold- and heat-sensitive TRP channels. *Nature* **2004**, *430*, 748–754. [CrossRef] [PubMed]
14. Bautista, D.M.; Siemens, J.; Glazer, J.M.; Tsuruda, P.R.; Basbaum, A.I.; Stucky, C.L.; Jordt, S.-E.; Julius, D. The menthol receptor TRPM8 is the principal detector of environmental cold. *Nature* **2007**, *448*, 204–208. [CrossRef]
15. Colburn, R.W.; Lubin, M.L.; Stone, D.J.; Wang, Y., Jr.; Lawrence, D.; D'Andrea, M.R.; Brandt, M.R.; Liu, Y.; Flores, C.M.; Qin, N. Attenuated cold sensitivity in TRPM8 null mice. *Neuron* **2007**, *54*, 379–386. [CrossRef]

16. Dhaka, A.; Murray, A.N.; Mathur, J.; Earley, T.J.; Petrus, M.J.; Patapoutian, A. TRPM8 is required for cold sensation in mice. *Neuron* **2007**, *54*, 371–378. [CrossRef] [PubMed]
17. Knowlton, W.M.; Bifolck-Fisher, A.; Bautista, D.M.; McKemy, D.D. TRPM8, but not TRPA1, is required for neural and behavioral responses to acute noxious cold temperatures and cold-mimetics in vivo. *Pain* **2010**, *150*, 340–350. [CrossRef]
18. Wang, S.; Lee, J.; Ro, J.Y.; Chung, M.-K. Warmth suppresses and desensitizes damage-sensing ion channel TRPA1. *Mol. Pain* **2012**, *8*, 22. [CrossRef]
19. Bandell, M.; Dubin, A.E.; Petrus, M.J.; Orth, A.; Mathur, J.; Hwang, S.W.; Patapoutian, A. High-throughput random mutagenesis screen reveals TRPM8 residues specifically required for activation by menthol. *Nat. Neurosci.* **2006**, *9*, 493–500. [CrossRef]
20. Wang, G. Ligand-stereoselective allosteric activation of cold-sensing TRPM8 channels by an H-bonded homochiral menthol dimer with head-to-head or head-to-tail. *Chirality* **2021**, *33*, 783–796. [CrossRef]
21. Brauchi, S.; Orio, P.; Latorre, R. Clues to understanding cold sensation: Thermodynamics and electrophysiological analysis of the cold receptor TRPM8. *Proc. Natl. Acad. Sci. USA* **2004**, *101*, 15494–15499. [CrossRef] [PubMed]
22. Yin, Y.; Zhang, F.; Feng, S.; Butay, K.J.; Borgnia, M.J.; Im, W.; Lee, S.-Y. Activation mechanism of the mouse cold-sensing TRPM8 channel by cooling agonist and $PIP_2$. *Science* **2022**, *378*, eadd1268. [CrossRef] [PubMed]
23. Jonstrup, A.T.; Fredsøe, J.; Andersen, A.H. DNA hairpins as temperature switches, thermometers and ionic detectors. *Sensors* **2013**, *13*, 5937–5944. [CrossRef] [PubMed]
24. Wang, G. The network basis for the structural thermostability and the functional thermoactivity of aldolase B. *Molecules* **2023**, *28*, 1850. [CrossRef]
25. Wang, G. Network basis for the heat-adapted structural thermostability of bacterial class II fructose bisphosphate aldolase. *ACS Omega* **2023**, *8*, 17731–17739. [CrossRef] [PubMed]
26. Wang, G. Thermal ring-based heat switches in hyperthermophilic class II bacterial fructose aldolase. *ACS Omega* **2023**, *8*, 24624–24634. [CrossRef] [PubMed]
27. Wang, G. Thermoring-Based Heat Activation Switches in the TRPV1 Biothermometer. *Int. J. Biol. Macromol.* **2023**, *248*, 125915. [CrossRef] [PubMed]
28. Wang, G. Thermoring basis for the TRPV3 bio-thermometer. *Sci. Rep.* **2023**, *13*, 21594. [CrossRef]
29. Floyd, R.W. Algorithm-97: Shortest Path. *Commun. Acm* **1962**, *5*, 345. [CrossRef]
30. Kiehna, S.E.; Waters, M.L. Sequence dependence of β-hairpin structure: Comparison of a salt bridge and an aromatic interaction. *Protein Sci.* **2003**, *12*, 2657–2667. [CrossRef]
31. Neel, A.J.; Hilton, M.J.; Sigman, M.S.; Toste, F.D. Exploiting non-covalent π interactions for catalyst design. *Nature* **2017**, *543*, 637–646. [CrossRef] [PubMed]
32. Fujita, F.; Uchida, K.; Takaishi, M.; Sokabe, T.; Tominaga, M. Ambient temperature affects the temperature threshold for TRPM8 activation through interaction of phosphatidylinositol 4,5-bisphosphate. *J. Neurosci.* **2013**, *33*, 6154–6159. [CrossRef]
33. Nadezhdin, K.D.; Neuberger, A.; Trofimov, Y.A.; Krylov, N.A.; Sinica, V.; Kupko, N.; Vlachova, V.; Zakharian, E.; Efremov, R.G.; Sobolevsky, A.I. Structural mechanism of heat-induced opening of a temperature-sensitive TRP channel. *Nat. Struct. Mol. Biol.* **2021**, *28*, 564–572. [CrossRef] [PubMed]
34. Kwon, D.H.; Zhang, F.; Suo, Y.; Bouvette, J.; Borgnia, M.J.; Lee, S.-Y. Heat-dependent opening of TRPV1 in the presence of capsaicin. *Nat. Struct. Mol. Biol.* **2021**, *28*, 554–563. [CrossRef] [PubMed]
35. Yudin, Y.; Lukacs, V.; Cao, C.; Rohacs, T. Decrease in phosphatidylinositol 4,5-bisphosphate levels mediates desensitization of the cold sensor TRPM8 channels. *J Physiol.* **2011**, *589*, 6007–6027. [CrossRef] [PubMed]
36. Xu, L.; Han, Y.; Chen, X.; Aierken, A.; Wen, H.; Zheng, W.; Wang, H.; Lu, X.; Zhao, Z.; Ma, C.; et al. Molecular mechanisms underlying menthol binding and activation of TRPM8 ion channel. *Nat. Commun.* **2020**, *11*, 3790. [CrossRef] [PubMed]
37. Ma, S.; Gisselmann, G.; Vogt-Eisele, A.K.; Doerner, J.F.; Hatt, H. Menthol derivative WS-12 selectively activates transient receptor potential melastatin-8 (TRPM8) ion channels. *Pak. J. Pharm. Sci.* **2008**, *21*, 370–378.
38. Chen, X.; Xu, L.; Zhang, H.; Wen, H.; Yang, F. Differential Activation of TRPM8 by the Stereoisomers of Menthol. *Front. Pharmacol.* **2022**, *13*, 898670. [CrossRef]
39. Gamper, N.; Shapiro, M.S. Target-specific PIP2 signalling: How might it work? *J. Physiol.* **2007**, *582*, 967–975. [CrossRef]
40. Matos-Cruz, V.; Schneider, E.R.; Mastrotto, M.; Merriman, D.K.; Bagriantsev, S.N.; Gracheva, E.O. Molecular Prerequisites for Diminished Cold Sensitivity in Ground Squirrels and Hamsters. *Cell Rep.* **2017**, *21*, 3329–3337. [CrossRef]
41. Pertusa, M.; Rivera, B.; González, A.; Ugarte, G.; Madrid, R. Critical role of the pore domain in the cold response of TRPM8 channels identified by ortholog functional comparison. *J. Biol. Chem.* **2018**, *293*, 12454–12471. [CrossRef] [PubMed]
42. Yang, S.; Lu, X.; Wang, Y.; Xu, L.; Chen, X.; Yang, F.; Lai, R. A paradigm of thermal adaptation in penguins and elephants by tuning cold activation in TRPM8. *Proc. Natl. Acad. Sci. USA* **2020**, *117*, 8633–8638. [CrossRef] [PubMed]
43. Bidaux, G.; Sgobba, M.; Lemonnier, L.; Borowiec, A.-S.; Noyer, L.; Jovanovic, S.; Zholos, A.V.; Haider, S. Functional and modeling studies of the transmembrane region of the TRPM8 channel. *Biophys. J.* **2015**, *109*, 1840–1851. [CrossRef] [PubMed]
44. Zhao, C.; Xie, Y.; Xu, L.; Ye, F.; Xu, X.; Yang, W.; Yang, F.; Guo, J. Structures of a mammalian TRPM8 in closed state. *Nat. Commun.* **2022**, *13*, 3113. [CrossRef] [PubMed]
45. Shimada, H.; Kusakizako, T.; Nguyen, T.H.D.; Nishizawa, T.; Hin, T.; Tominaga, M.; Nureki, O. The structure of lipid nanodisc-reconstituted TRPV3 reveals the gating mechanism. *Nat. Struct. Mol. Biol.* **2020**, *27*, 645–652. [CrossRef] [PubMed]

46. Taberner, F.J.; López-Córdoba, A.; Fernández-Ballester, G.; Korchev, Y.; Ferrer-Montiel, A. The region adjacent to the C-end of the inner gate in transient receptor potential melastatin 8 (TRPM8) channels plays a central role in allosteric channel activation. *J. Biol. Chem.* **2014**, *289*, 28579–28594. [CrossRef] [PubMed]
47. Fernández, J.A.; Skryma, R.; Bidaux, G.; Magleby, K.L.; Scholfield, C.N.; McGeown, J.G.; Prevarskaya, N.; Zholos, A.V. Voltage- and cold-dependent gating of single TRPM8 ion channels. *J. Gen. Physiol.* **2011**, *137*, 173–195. [CrossRef]
48. Sisco, N.J.; Helsell, C.V.M.; Van Horn, W.D. Competitive Interactions between PIRT, the Cold Sensing Ion Channel TRPM8, and PIP2 Suggest a Mechanism for Regulation. *Sci. Rep.* **2019**, *9*, 14128. [CrossRef]